Origin of High Activity and Selectivity of CuO/CeO₂ Catalysts Prepared by Solution Combustion Synthesis in CO-PROX Reaction

P.S. Barbato[1], S. Colussi[2], A. Di Benedetto[3], G. Landi[1*], L. Lisi[1], J. Llorca[4], A. Trovarelli[2]

[1]Research Institute on Combustion-CNR, Naples, Italy

[2]Dipartimento Politecnico, Università di Udine, Udine, Italy

[3]Dipartimento di Ingegneria Chimica, dei Materiali e della Produzione Industriale, Univ. of Naples Federico II, Naples, Italy

[4]Institut de Tècniques Energètiques and Centre for Research in Nanoengineering, Universitat Politècnica de Catalunya, Barcelona, Spain

[*]corresponding author: landi@irc.cnr.it; phone: +39 0817682235.

Abstract

A CuO/CeO₂ catalyst with 4 wt% CuO nominal content has been prepared by Solution Combustion Synthesis (SCS) and characterized by ICP-MS, BET surface area analysis, XPS, HRTEM, H_2 and CO TPR. The catalyst, showing a rather homogenous distribution of copper that strongly interacts with ceria, has been tested in CO-PROX reaction also in the presence of CO_2 and H_2O. The enhanced performance of the catalyst compared to that of an impregnated sample with the same copper loading has been explained by modelling experimental CO_2 TPD curve, which allowed the determination and quantification of different active sites. The temperature range of activity and the ratio of the amount of sites activating CO and H_2 oxidation respectively, estimated for the two catalysts through the model, explain the superior performance of the sample prepared by SCS despite its lower surface area.

1. Introduction

The hydrogen production from hydrocarbons for PEMFC application requires a purification stage to abate the residual CO concentration in the H_2-rich streams coming from the water gas shift step. For this purpose copper-ceria catalysts have been extensively investigated as possible substitute of precious metals, due to their lower cost and comparable or even higher activity for CO selective oxidation[1-8]. The good performances of this class of materials have been related to the synergistic interaction between copper and cerium oxide, since the activity towards CO oxidation has been essentially ascribed to the copper oxide-ceria interfacial sites[1-13]. In particular, it has been proposed that Cu^{2+} entities strongly interacting with ceria are responsible for the enhanced ceria-promoted reduction of dispersed CuO upon contact with the reaction mixture. In addition, the activity of such materials depends on copper oxide dispersion and/or on the extent of interaction with ceria.

The presence of Cu^{1+} species stabilized through the interaction with cerium oxide has also been suggested[14-18]; accordingly, the reaction path is assumed to follow a redox mechanism, involving the change of the oxidation state of both copper ($Cu^{2+} \leftrightarrow Cu^{1+}$) and cerium ($Ce^{4+} \leftrightarrow Ce^{3+}$)[3, 6, 14-15].

Copper dispersion and interaction with ceria are affected by the catalyst preparation method[2, 9, 19-25]. Tang et al.[9] studied the redox properties of CuO/CeO_2 catalysts prepared by wet impregnation, co-precipitation and deposition-precipitation. The authors found a correlation between the catalyst performances, in terms of activity and redox properties, and the preparation method. They found that the catalysts prepared by co-precipitation method had the best catalytic activity due to a more uniform dispersion and a stronger interaction between copper species and ceria.

Likewise Sedmak et al.[2] and Avgouropoulos et al.[20] reported that the highest degree of interaction between CuO and CeO_2 is achieved in co-precipitated samples compared to catalyst prepared by sol-gel methods, while the catalysts prepared via co-precipitation and impregnation showed lower catalytic performances with respect to that prepared via citrate-hydrothermal and urea combustion methods. On the contrary, in the work of Gurbani et al.[23] the catalyst prepared by sol-gel technique showed performance slightly better than that prepared by urea combustion synthesis. Moreover,

these samples were significantly more active than a co-precipitated sample, but less active than an impregnated one. Also Yang et al.[19] investigated the effect of the preparation method on the performances of CuO/CeO_2 catalysts in the complete methane combustion. The catalysts were synthesized by sol-gel, hydrothermal and nitrate thermal decomposition methods. They found that the preparation method of CeO_2 has a great influence on the physicochemical properties and activities of CuO/CeO_2 catalysts concluding that the catalyst prepared via nitrate thermal decomposition showed the highest surface area, the smallest particle size, the highest dispersion of copper species and strong metal-support interaction, resulting in the highest activity for methane combustion.

The enhanced performance of catalysts prepared by methods promoting copper-ceria interaction, such as sol-gel, co-impregnation, urea gelation or urea nitrate combustion are also reported by Rattan et al.[21] for CO oxidation and Mishra et al.[22] for complete oxidation of n-hexane and iso-octane. Good metal dispersion and improved interaction with ceria in CO-PROX catalysts prepared by SCS have been reported for copper[23, 25, 26] and PGM[27].

Therefore, from previous investigations it turns out that a suitable choice of the preparation method markedly affects the copper-ceria interactions. Nevertheless, a quantitative analysis of the extent of this phenomenon has never been performed.

In a previous work[28] we showed that it is possible to use a technique based on the combined experimental and kinetic modelling of the temperature programmed desorption of CO_2 (TPD) from CuO/CeO_2 catalysts to identify the sites activating CO and H_2 oxidation. With the aid of this analysis we were able to identify and quantify the concentrations of bulk-like copper oxide species responsible for H_2 oxidation which increased with copper loading[28].

In this work we applied this combined (experimental/modelling) technique, called Kinetically Modelled Temperature Programmed Desorption (KM-TPD), to identify and to quantify the active sites of two copper-ceria catalysts with the same copper content prepared by two different methods: solution combustion synthesis (SCS), that is supposed to promote a very good interaction between

copper and CeO_2, and the wet impregnation, which typically provides a copper dispersion lower than SCS, especially when approaching or exceeding the mono-layer coverage.

The performances of the two catalysts in CO-PROX reaction were evaluated in order to correlate catalytic activity with active sites identified through the KM-TPD. To support our findings, the catalysts were characterized by X-ray diffraction analysis (XRD), BET surface area measurements, ICP-MS, X-ray photoelectron spectroscopy (XPS), high resolution transmission electron microscopy (HRTEM) and H_2 and/or CO Temperature Programmed Reduction.

2. Experimental

2.1 Catalyst preparation

Solution combustion synthesized sample (CuCe-S) with nominal 4 wt % CuO was prepared by one-step solution combustion synthesis (SCS), using $Cu(NO_3)_2·2,5H_2O$ (Aldrich, 99,99%) and $(NH_4)_2Ce(NO_3)_6$ (Treibacher Industrie A.G., Austria) as oxidizers, and oxalyldihydrazide ($C_2H_6N_4O_2$, ODH) as the reducing agent. For the synthesis, about 10 g of ceric ammonium nitrate was used, with the suitable amount of copper nitrate to obtain the final 4 wt% CuO loading. The amount of fuel was chosen in order to balance the oxidizing valency of the reagents, according to the standard SCS procedure[29]. The precursors and the fuel (ODH) were dissolved in about 50 ml of distilled water, and the solution was put into a preheated furnace in static air at 380 °C, where the combustion took place with complete evaporation of water leading to a fine powder product. After combustion, the powder so obtained was removed from the furnace and left to cool at room temperature. The sample was then calcined in air at 450°C for 2h.

The reference sample (CuCe-I) with nominal 4 wt % CuO was prepared by wet impregnation using an aqueous solution containing copper acetate (Aldrich) as precursor and CeO_2 (56 m^2/g), kindly provided by GRACE, as support. Impregnation was carried out in a rotating evaporator at 50 °C, 90 mbar and with a velocity of 120 rpm.The sample was dried overnight at 120°C. Finally, the CuCe-I was calcined at 450°C for 2h, in order to obtain the active copper oxide phase.

2.2 Catalyst characterization

The actual metal content was determined by ICP-MS analysis using an Agilent 7500CE instrument. BET surface areas (SSA) of supports and catalysts were measured by N_2 adsorption at 77K with a Quantachrome Autosorb-1C instrument after degassing the samples at 150°C for 1.5 h.

X-ray diffraction spectra were collected with a Philips X'Pert diffractometer equipped with an X'Celerator detector with Cu-K_α radiation. The measurements were carried out with a step size of 0.02° and a counting time of 80s per step. X-ray photoelectron spectroscopy (XPS) was performed with a SPECS system equipped with an Al anode XR50 source operating at 150 W and a Phoibos 150 MCD-9 detector. Spectra were recorded with pass energy of 25 eV at 0.1 eV steps at a pressure below $5 \cdot 10^{-12}$ bar. Binding energies were referred to the adventitious C 1s signal at 284.8 eV.

Fresh and used samples for HRTEM studies were mounted on standard grids with a holey-carbon film. A JEOL JEM 2010F microscope with a field emission gun (200 kV, 0.19 nm point-to-point resolution) was used for microstructural characterization.

Temperature Programmed Reduction (TPR) analysis was carried out in a quartz fixed bed reactor using mixtures of 2 vol.% H_2 and/or 1 vol.% CO in N_2 with a total flow rate of 14 l(STP)/h, loading 0.3 g sample with a particle dimension of 180-300 μm. In all TPR tests the reactor was heated at 10°C/min up to 450°C, maintaining the final temperature for 1h. Hydrogen and carbon monoxide uptakes and CO_2 production were monitored using a Fisher-Rosemount NGA2000 continuous analyzer set up to measure CO (NDIR detector), CO_2 (NDIR detector), H_2 (TC detector) and O_2 (paramagnetic detector) concentrations.

2.3 Activity tests

The lab-scale set-up used for CO-PROX experiments was described elsewhere[28]. The powder catalyst (300 mg) with 180-300 μm particle size was placed in a tubular quartz reactor. A thermocouple placed inside a tube co-axial with the reactor provided the measurement of the catalyst temperature. The reactor was placed into an electric tubular furnace (Lenton) provided with

a PID-type controller. An ice bath based condenser and a $CaCl_2$ trap were used to dry the gaseous flow downstream to the reactor; the dried flow was analyzed by the gas analysis system described in the section 2.2.

Catalytic tests were conducted at fixed flow rate (20 l(STP)/h); as a consequence contact time, defined as the (catalyst weight)/(flow rate) ratio, was equal to 0.054 $g \cdot s/(cm^3)$. Hydrogen, carbon monoxide and oxygen concentrations were set at 50 vol.%, 0.5 vol.% and 0.9 vol.%, respectively. Reaction temperature ranged from 80 to 200 °C to explore the whole temperature range of interest for CO-PROX. Mass balance was always closed within ±4%. Reactants conversions and selectivity of oxygen reacting with carbon monoxide were calculated according to the following equations:

$$x_{CO} = \frac{CO^{IN} - CO^{OUT}}{CO^{IN}} \qquad (1)$$

$$x_{O_2} = \frac{O_2^{IN} - O_2^{OUT}}{O_2^{IN}} \qquad (2)$$

$$x_{H_2} = \frac{H_2^{IN} - H_2^{OUT}}{H_2^{IN}} \qquad (3)$$

$$s_{CO} = \frac{\Delta O_2^{CO}}{\Delta O_2^{CO} + \Delta O_2^{H_2}} = 0.5 \cdot \frac{CO^{IN} - CO^{OUT}}{O_2^{IN} - O_2^{OUT}} \qquad (4)$$

where x_{CO}, x_{O2}, x_{H2} and s_{CO} are, respectively, the CO, O_2 and H_2 conversions and the O_2 selectivity to CO_2 and ΔO_2^{CO} and $\Delta O_2^{H_2}$ the oxygen moles consumed for CO and H_2 oxidation, respectively.

2.4 Kinetically Modelled Temperature Programmed Desorption (KM-TPD) of CO_2

KM-TPD is a combined experimental/modelling technique, here applied to CO_2 desorption.

CO_2 Temperature Programmed Desorption (TPD) tests were carried out by using a Micromeritics Autochem II 2020 analyzer. About 100 mg sample was pre-treated 1 h at 450°C in flowing air and

then contacted for 45 min at room temperature with a 15 vol.% CO_2/He mixture. After 30 min He purging, the sample was heated at 10°C/min up to 300°C. A TC detector was used to monitor the CO_2 evolution.

A TPD kinetic model was used to identify the number and type of CO_2 species adsorbed on the catalyst surface and to quantify their amounts.

In Di Benedetto et al.[28] more details about the governing equations and approximations used in the model are reported.

Briefly, the model assumes that CO_2 is adsorbed over several catalytic sites (σ_1, σ_2, …σ_n, with $n \leq 4$), which do not interact with each other, giving rise to CO_2-σ_i species whose fractions with respect to the total number of sites are indicated as θ_i.

The unsteady state balances on the fractions are the following:

$$\frac{d\theta_i}{dt} = -k_i^o exp\left(-\frac{Edes_i}{RT}\right)\vartheta_i^{ni} \quad \text{for i=1 to n} \tag{5}$$

where $k_i°$, $E_{des\ i}$ and n_i are the kinetic constant, the activation energy and the reaction order for CO_2 desorption from site σ_i.

The initial conditions read:

$$t = 0; \theta_{I} = \theta^0_i \text{ for } i = 1 \text{ to } n \tag{6}$$

The TPD cell was modelled as a perfectly mixed reactor due to the very low value of the axial Pe number (Pe = 0.007).

Accordingly, the CO_2 molar balance is the following:

$$\frac{1}{C^0}\frac{dC_{CO2}}{dt} - \frac{C_{CO2}}{C^0\tau} = \sum_{i=1}^{n} k_i^o exp\left(-\frac{Edes_i}{RT}\right)\vartheta_i^{ni} \tag{7}$$

The initial condition is the following:

$$t = 0; C_{CO2} = 0 \tag{8}$$

where C_{CO2} is the CO_2 concentration and $C°$ is the total gas concentration in mol/m^3 and τ is the residence time (s).

As in the TPD experiment, the temperature (T) increase with time is linear:

$$T = T^o + \beta t \hspace{10cm} (9)$$

where $\beta = 10$ °C/min.

The model parameters are k°_i, $E_{des\,i}$ and θ^0_i which were computed by solving the model and fitting the curves with the experimental curves. The n value was fixed as equal to the values obtained for the impregnated sample. We started from the values of the impregnated sample.

The system of equations 5-7 with the initial conditions (6 and 8) was solved by means of the Runge-Kutta method.

The root mean square error SRMSE normalized by the maximum value of the TPD curve (TPD_{max}) was computed to evaluate the differences between the experimental and the model TPD curves:

$$SRMSE = \frac{1}{TPD_{max}} \sqrt{\frac{1}{N} \sum_{i=1}^{N} (TPDexp(i) - TPDmodel(i))^2} \hspace{5cm} (10)$$

According to Kanervo et al.[30], if the SRMSE is less than 0.045 then the curves may be considered in good agreement.

3. Results

3.1 Textural and structural characterization

The copper content of the fresh catalysts is reported in Table 1. Both samples have a metal content close to the nominal one, within the experimental error. Analyses of used samples (not reported) were also performed and no significant differences were found.

Table 1. Characteristics of Cu-based catalysts

Sample	Actual CuO content, wt.%	SSA, m²/g	Particle size (nm)
CuCe-I	4.2	45	13
CuCe-S	3.9	15	45

The lower surface area of the SCS sample (Table 1) is due to the high temperature reached during the combustion step and is typical of the samples prepared by this method.[23, 26-27]

The XRD pattern of CuCe-I sample has been previously reported.[31] The diffraction peaks can be assigned to cubic ceria (JCPDS 75-0076) without evidence of the presence of CuO or Cu_2O phases for both samples. The absence of diffraction signal from CuO is in agreement with previous investigations[25], although CuO particles were detected by XRD in catalysts with a larger copper amount[23]. The crystallite size of ceria particles, as calculated by means of Scherrer's equation, is very different between the two samples (Table 1); for CuCe-S (45 nm) a certain growth of ceria crystallites is evident and it is due to the high temperature reached during the combustion synthesis, in accordance to its lower surface area.

3.2 XPS and HRTEM results

The surface atomic Cu/Ce ratios obtained by XPS analysis are reported in Table 2. Both fresh samples show a similar Cu concentration at the surface, although a higher Cu surface concentration would be expected for the SCS catalyst taking into account the lower surface area of this sample compared to that of CuCe-I. This suggests that the SCS technique promotes a more uniform distribution of copper, being likely partially included into the ceria structure similarly to what observed on other CuCe samples made by SCS[32]. Nevertheless, a strong copper surface enrichment was observed for CuCe-S after reaction, not occurring for CuCe-I, which accounts for a copper surface segregation under reaction conditions. Also, the Cu(II) satellite lines in the Cu 2p XP spectra of the CuCe-S sample become more intense after reaction, providing additional evidence for the formation of segregated Cu oxide at the surface (Figure 1).

Table 2. Cu/Ce atomic ratios calculated by XPS analysis on as prepared and used samples

Sample	Cu/Ce
CuCe-I fresh	0.21
CuCe-I used	0.24
CuCe-S fresh	0.26
CuCe-S used	0.55

Figure 2a shows an HRTEM image of CuCe-S. The sample is dominated by large, irregular CeO_2 crystallites of about 50-150 nm. A representative high resolution image is depicted in Figure 2b. Lattice fringes at 3.12 Å correspond to the (111) plane of CeO_2. This value is similar to the one expected for pure CeO_2, thus the incorporation of large quantities of Cu into the CeO_2 lattice is not likely to occur but the inclusion of some Cu atoms into ceria lattice cannot be ruled out. On the other hand, no superstructure is visible and no particles of CuO or Cu_2O are distinguished on the surface of CeO_2 crystallites, (according to the collected XRD spectra) thus indicating that (i) Cu may be indeed inside the CeO_2 lattice or, alternatively, (ii) Cu is extremely dispersed. The former explanation is in line with the XPS results showing that some of the Cu is likely included into the CeO_2 lattice. In Figure 2b, some higher electron contrast spots are marked by arrows. They are at the sub-nanometer level and might correspond to Cu oxide, but this should be considered at the limit of the technique.

Figures 3a and 3b show the CuCe-S sample after reaction. In this case, higher electron contrast particles of about 1-2 nm are clearly visible, likely corresponding to Cu oxide. It is not possible to infer the nature of Cu oxide because those particles do not exhibit lattice fringes (due to their small size), thus again supporting the hypothesis of a good copper dispersion. Figure 3b shows a single particle of about 1.5 nm on top of ceria. Interestingly, after reaction, Cu oxide particles are found in profile view in the sample, thus demonstrating that Cu oxide is on the surface. This is in agreement with the XPS results, showing that the Cu/Ce ratio increases strongly after reaction.

The HRTEM images of the CuCe-I sample have been already reported and discussed previously.[30] The sample is comprised by ceria crystallites of about 6-10 nm in size. This value agrees very well with XRD analysis. Several CuO particles are recognized in the HRTEM images with a dimension around 5-8 nm[31]. HRTEM images of CuCe-I after reaction show no differences compared to the fresh catalyst.

3.3 Temperature Programmed Reduction.

The redox properties of the catalyst prepared by SCS have been investigated by H_2 and CO-TPR. These species, with different reducing properties, are also those in competition in the CO-PROX reaction. The different affinity of the catalytic sites towards CO and H_2 has been also investigated by co-feeding CO (1 vol.%) and H_2 (2 vol.%) during TPR tests.

3.3.1 H_2-TPR

In Figure 4, the H_2-TPR profiles of CuCe-S and CuCe-I catalysts are compared. Profiles obtained by repeating TPR experiments after re-oxidation do not show significant differences. The H_2-TPR pattern of the CuCe-S catalyst is characterized by 2 peaks at about 140°C and 180°C. CuCe-I shows a more complex TPR profile, in which three well detectable peaks and a shoulder can be detected. Moreover, in the case of the impregnated sample, the reduction by hydrogen starts at a temperature below that of CuCe-S catalyst.

In Table 3 the total hydrogen uptakes together with the molar ratios between hydrogen and copper are reported. The values of hydrogen uptake are 601 and 784 µmol/g for CuCe-S and CuCe-I, respectively. As typically observed in copper ceria catalysts[1, 33], the H_2 consumption is higher than the stoichiometric ratio for the reduction of Cu^{2+} to Cu^0 that in this case corresponds to about 500 µmol/g. As a consequence, also in the case of CuCe-S it could be inferred that the reduction of some ceria particles promoted by copper takes place. However, it should be underlined that the reduction degree of the CuCe-S sample is significantly lower than that obtained on CuCe-I catalyst, indicating a higher degree of interaction between hydrogen and the impregnated sample, which could explain its lower selectivity in the reaction.

Table 3. Overall H_2 and CO uptakes and relative (reducing agent)/Cu ratios obtained by TPR on CuCe-S and CuCe-I.

Reducing agent	M^a	CuCe-S		CuCe-I	
		Uptake^b	M^a/(Cu)	Uptake^b	M^a/(Cu)
H_2	H_2	601	1.19	784	1.49
CO	CO	724	1.44	894	1.70
H_2 + CO	H_2	157	0.31	n.v.^{c}	-
	CO	453	0.90	814	1.55

^{a}Molecule = H_2; CO.
^{b} μmol g^{-1}
^{c} negative value

3.3.2   CO-TPR

CO TPR profiles are shown in Figure 5 (a and b) for CuCe-S, and in Figure 5c for CuCe-I. As evident from Figure 5a, CO uptake not associated to a simultaneous CO_2 evolution takes place on CuCe-S at room temperature, as already reported for the copper ceria systems[33, 34]. However, CO_2 production slightly overcomes the CO uptake in the low temperature region (<100°C) (Figure 5b); thus, it could be argued that the CO_2 formed but not desorbed at room temperature, when the first CO consumption occurs, starts to evolve at this temperature range. At temperatures higher than 120°C, CO and CO_2 profiles overlap, with a major peak at approximately 190°C (Figure 5b). This behavior is different from that of CuCe-I in which, as previously reported[33] and shown in Figure 5c, the CO_2 emission is higher than CO consumption in a wider range of temperature. Moreover, also for CO TPR, it should be observed the lower complexity of the TPR curve of the SCS catalyst compared to the impregnated sample, suggesting a more uniform composition and homogeneous distribution of CuCe-S.

The total CO uptake value is higher than that of H_2, probably accounting for a larger participation of promoted ceria in the reduction by CO (see Table 3). The values of CO uptake at RT obtained by integrating the CO signal for ten minutes and subtracting the reactor hold up are reported in Table 4. This value is equal to 99 μmol/g for CuCe-S and is obtained after three TPR cycles (with sample re-oxidation between reduction cycles), remaining constant after further reduction. The starting value,

i.e. the CO uptake of the fresh sample, was 81 µmol/g. Since it is expected that the CO uptake at RT is attributable only to copper surface species[33], its progressive increase with TPR cycles suggests a superficial copper enrichment, due to copper surfacing and/or re-dispersion, obtained upon interaction of the sample with CO. As reported previously, no differences are detected by repeating H_2-TPR. These evidences suggest that the higher Cu/Ce ratio calculated by XPS analysis of the sample after reaction is more likely attributable to the exposure to CO rather than to H_2.

Table 4. Partial H_2 and CO uptakes and relative (reducing agent)/Cu ratios obtained by TPR on CuCe-S and CuCe-I.

Reducing agent	Final T, °C	M[a]	CuCe-S		CuCe-I	
			Uptake[b]	M[a]/(Cu)	Uptake[b]	M[a]/(Cu)
CO	25	CO	99	0.20	163	0.31
H₂ + CO	25	H₂	-	-	-	-
		CO	86	0.17	146	0.28
H₂ + CO	200	H₂	118	0.23	217	0.41
		CO	383	0.76	609	1.16

[a] Molecule = H_2; CO.
[b] µmol g^{-1}

3.3.3 H₂-CO TPR

The TPR profiles of CuCe-S obtained by co-feeding H_2 and CO and the quantitative data evaluated from the integration of the curves are reported in Figure 6a and in Tables 3 and 4, respectively.

As for CO-TPR, some CO adsorption takes place at RT with a slightly lower amount than that detected during CO TPR (Table 4). Moreover, the CO uptake at higher temperature shows two peaks at 78°C and 164°C respectively (Figure 6a). The high temperature signal is sharper compared to that corresponding to CO-TPR and a well-defined low temperature peak appears. The signal of H_2 uptake has only one peak, approximately centered in correspondence of the main peak of CO signal, but with a lower intensity. Moreover, at T>200°C the H_2 baseline below zero accounts for a small production of H_2, which could be related to the occurrence of the Water Gas Shift (WGS) reaction between CO and surface hydroxyl groups.[35] Although the behavior of CuCe-I (Figure 6b) is similar to that of CuCe-S, a more pronounced CO_2 fraction is released at low temperatures on

CuCe-I, and the hydrogen consumption is significantly higher. Finally, hydrogen production through WGS with surface hydroxyl groups is more evident over CuCe-I.

In Table 3 the $H_2(CO)/Cu$ ratios are reported. As expected, the CO/Cu and H_2/Cu ratios are lower than those obtained when feeding a single reductant, while the overall degree of reduction is closer to that obtained during H_2 TPR. Nevertheless, the decrease of the H_2/Cu ratio is more pronounced than that of CO/Cu ratio ((CO/Cu)/(H_2/Cu) $\approx$ 3 in co-feeding TPR, (CO/Cu)/(H_2/Cu) $\approx$ 1,2 in the case of single feeding), indicating that the catalyst reacts preferentially with CO when both molecules are present.

As it appears from Table 4, the value of the total hydrogen uptake evaluated for CuCe-S up to 200°C, although higher than the stoichiometric ratio for the reduction of Cu^{2+} to Cu^0, is lower than that reported for the CuCe-I sample. As a consequence, also in the simultaneous H_2-CO TPR it could be inferred that for CuCe-S the reduction of ceria promoted by copper takes place to a lower extent compared to the impregnated catalyst. Martìnez-Arias et al.[36] also observed a lower H_2/Cu ratio from their TPR experiments carried out on copper-ceria catalysts prepared by techniques that promote copper inclusion into ceria lattice compared to the impregnated samples. They suggested that this copper incorporation decreased to some extent the reducibility of copper. As a matter of fact, the ceria reduction is likely promoted by surface copper, and the lower reduction degree of CuCe-S is attributable to a greater copper/ceria mixing and, consequently, to a lower fraction of copper located at the surface, which in turn is higher for the impregnated catalyst.

We can conclude that, as found for the impregnated CuO/CeO_2 catalysts,[33] the CO/Cu ratio found in CO-TPR over the SCS sample exceeds the stoichiometric ratio, and the values are higher than those found for H_2/Cu in H_2-TPR. This result suggests that the catalyst has a stronger affinity towards CO than toward H_2. Nevertheless, it is worth noting that the ratio between CO and H_2 uptake for the two catalysts is higher over the CuCe-S sample, especially when CO and H_2 are co-fed, confirming that the CuCe-S catalyst could exhibit a higher selectivity than CuCe-I.

3.4 Activity results

Figure 7 shows the CO conversion and selectivity as a function of temperature for SCS and impregnated catalysts. Both conversion and selectivity are higher in the whole range of temperature for CuCe-S with respect to CuCe-I. This result is quite surprising if we take into account that the CuCe-S catalyst exhibits a SSA equal to one third of the reference sample; however it can be partially related to the high Cu enrichment of the CuCe-S surface, as evidenced by XPS measurements. This is also in line with the higher activity of samples prepared by solution combustion synthesis as observed in other catalytic reactions.[32, 37]

In particular, complete CO conversion is reached with CuCe-S sample already at 140°C with selectivity approximately equal to 80%. At the same temperature, the reference sample shows 90% conversion with selectivity below 60%.

These results are also in line with the H_2 TPR measurements showing a higher affinity of the impregnated sample towards H_2, with a CO-PROX selectivity never reaching 100% also at the lowest temperature, suggesting that H_2 oxidation is activated at rather low temperature.

The stability of CuCe-S catalyst under reaction conditions was also investigated (Figure 8). The test was carried out at 80°C. A progressive decrease of CO concentration at the reactor outlet was measured in the first thirty minutes of reaction and no deactivation was observed after 45h run. This behavior is different from that reported for the impregnated sample, showing stable operation for tens of hours but after a deactivation detected during the first hours[28]. The initial activation of CuCe-S catalyst, evidently related to the increase of the amount of the active sites, could be likely related to a slow surfacing of copper initially incorporated into the structure, as observed by XPS analysis, which makes more and more copper available for CO oxidation at the beginning of reaction.

3.5 CO$_2$ KM-TPD results

In our previous works we demonstrated that different catalytic sites could be titrated by CO$_2$ for catalysts prepared by wet impregnation with different copper concentration[28] or supported on a Fe-promoted ceria.[38] In those studies we showed that three different sites can be identified through CO$_2$ adsorption on copper/ceria catalysts. These sites were associated to i) cerium centers deeply modified by the strong interaction with copper and active towards CO oxidation, ii) unmodified cerium centers and iii) copper centers in supported copper oxide active for H$_2$ oxidation. These sites are named as θ_{Ce1}, θ_{Ce2} and θ_{Cu};[38], respectively. The different values of θ_{Ce1}, θ_{Ce2} and θ_{Cu} can explain the different performances of different catalysts in CO-PROX. Thus, here we use this technique to obtain information about sites distribution in the SCS material in order to verify if this technique can identify and quantify catalytic sites also when a different distribution is induced by the preparation method.

The CO$_2$-TPD profile of CuCe-I has been already discussed in Di Benedetto et al..[28] For the sake of comparison, the CO$_2$-TPD signal collected for CuCe-I both per weight of catalyst and per surface area is reported in Figure 9 a and b respectively, together with that of CuCe-S. The shape of the two curves is similar showing a main peak at about the same temperature and a long tail, although a shoulder clearly appears only for CuCe-I. Due to the lower SSA an inversion of the area of TPD curves is observed (confirmed by quantitative data reported in Table 5) when results are given per surface area, indicating that CuCe-S has a higher intrinsic capacity to adsorb CO$_2$. Moreover, the comparison between these two profiles evidences a slightly higher contribution at low temperature for CuCe-S.

As outlined in the experimental section, CO$_2$ TPD profiles were modelled according to Polanyi-Wigner equation under the Redhead approximation based on non-interacting catalytic sites. The model equations describe CO$_2$ desorption from the different sites as discussed in Di Benedetto et al..[28] CO$_2$ TPD profile of CuCe-I was reproduced assuming the presence of three kinds of sites; the

same was found for the SCS sample and for both catalysts the SRMSE parameter ≤ 0.045[30] (see Table 6) indicated a good agreement between experimental and calculated curves.

In Table 6 the kinetics parameters of CO_2 desorption steps are reported. The SCS sample has lower initial values of all sites (θ^0) and a lower value of the activation energy of CO_2 desorption from the sites previously associated to CO-oxidation centers (θ_{Ce1})[28]. The ratio between the $\theta°_{Ce1}$ values of the impregnated and SCS samples (0.36 and 0.175, respectively) is the same of the ratio of the CO uptakes at RT (163 µmol/g and 81 µmol/g, respectively) suggesting that these sites are those able to adsorb and likely even oxidize CO at temperatures as low as RT, desorbing CO_2 at higher temperature. The lower desorption energy associated to these sites could be related to the high activity even at very low temperature exhibited by CuCe-S, despite of the lower surface area, which likely promotes an easier CO_2 desorption thus making available more CO oxidation sites. Moreover, the ratio of θ_{Cu} sites of CuCe-I and CuCe-S, associated with H_2 oxidation, is more than 3 and this well explains the higher selectivity of CuCe-S.

This is more evident if we observe the CO_2 desorbed from each site as a function of temperature for CuCe-I and CuCe-S reported in Figure 10, and the corresponding percentage fraction reported in Table 5. First of all, the distributions obtained are in agreement with the results of H_2 and CO TPR, which suggest a more homogeneous nature of copper sites for CuCe-S catalyst. In fact this sample shows a clear predominance of CO oxidation sites with respect to other sites, while on CuCe-I a comparable amount of CO and H_2 oxidation sites is detected.

Moreover, the H_2 oxidation sites identified for SCS sample entail that CO oxidation can proceed up to higher temperature before H_2 oxidation starts compared to CuCe-I catalyst. Indeed, up to 130-140°C desorption of CO_2 (both fed and produced by CO oxidation) from CO oxidation sites remarkably prevails for CuCe-S catalyst, whereas such difference cannot be detected for CuCe-I, thus explaining why this sample does not reach 100% selectivity even at low temperature.

Finally, according to the CO_2 TPD model, the involvement of H_2 oxidation sites at 100°C is limited for CuCe-S sample whereas it is significant for CuCe-I catalyst; this means that CO oxidation has a

larger O_2 availability in the low temperature range for the former catalyst thus leading to its higher activity and selectivity.

Table 5. Amount of CO_2 desorbed during TPDs of CuCe-S and CuCe-I (both per sample weight and per surface area) and amounts of CO_2 calculated for the different sites as obtained by TPD modeling (both as absolute amount and as percentage of the total amount).

Sample	Desorbed CO_2 $\mu mol\ g^{-1}$	Desorbed CO_2 $\mu mol\ m^{-2}$	CO_2 desorbed from θ_{Ce1} $\mu mol\ g^{-1}$	%	CO_2 desorbed from θ_{Ce2} $\mu mol\ g^{-1}$	%	CO_2 desorbed from θ_{Cu} $\mu mol\ g^{-1}$	%
CuCe-I	296	6.58	130	*43.8*	28.4	*9.6*	138	*46.6*
CuCe-S	122	8.14	67	*55.0*	5.7	*4.7*	49	*40.3*

Table 6. Values of the kinetic parameters for CuCe-S and CuCe-I catalysts.

Sample	θ_{Ce1}				θ_{Ce2}				θ_{Cu}				
	$\theta°$	$E_{des}{}^a$	k^{ob}	n	$\theta°$	$E_{des}{}^a$	k^{ob}	n	$\theta°$	$E_{des}{}^a$	k^{ob}	n	SRMSE
CuCe-I	0.36	47320	$1.1\ 10^6$	1	0.08	51500	$1.4\ 10^5$	1	0.40	39034	$1.0\ 10^5$	2	0.0305
CuCe-S	0.175	46000	$1.1\ 10^6$	1	0.015	51500	$1.4\ 10^5$	1	0.128	39034	$1.0\ 10^5$	2	0.013

[a] J mol^{-1};
[b] min^{-1}.

4. Conclusions

A technique based on the combined experimental and modelling of the temperature programmed desorption of CO_2 (Kinetically Modelled Temperature Programmed Desorption, KM-TPD) has been applied to determine the sites distribution of a copper ceria catalyst with a nominal content of 4 wt% CuO prepared by solution combustion synthesis and to explain its enhanced performance in CO-PROX compared to an analogous conventional catalyst prepared by wet impregnation.

The whole results showed that this SCS sample is characterized by a stronger interaction between copper and CeO_2, suggesting a significant copper incorporation into CeO_2 lattice and a good copper

dispersion on the catalyst surface. Modelling of CO_2 TPD profiles led to determine a more homogeneous copper sites distribution for the catalyst prepared by SCS with a large dominance of sites ascribable to CO oxidation. On the other hand, the significant overlapping of the temperature range associated to sites activating both CO and H_2 oxidation evaluated for the impregnated catalyst and the lower ratio of their relevant amount is the reason of the worse performance of this sample in CO-PROX under standard reaction conditions (absence of CO_2 and H_2O in the feed). The limited contribution to H_2 oxidation for the catalyst prepared by SCS gives rise to a larger O_2 availability in the low temperature range leading to both higher activity and selectivity. As a consequence, although with a markedly lower surface area, this catalyst shows superior performance compared to the impregnated sample.

Acknowledgments

References

[1] Martínez-Arias, A.; Fernández-García, M.; Gálvez, O.; Coronado, J. M.; Anderson, J. A.; Conesa, J. C.; Soria, J.; Munuera, G. Comparative Study on Redox Properties and Catalytic Behavior for CO Oxidation of CuO/CeO_2 and $CuO/ZrCeO_4$ Catalysts. *J. Catal.* **2000**, *195*, 207-216.

[2] Sedmak, G.; Hocevar, S.; Levec, J. Kinetics of Selective CO Oxidation in Excess of H_2 over the Nanostructured $Cu_{0.1}Ce_{0.9}O_{2-y}$ Catalyst. *J. Catal.* **2003**, *213*, 135-150.

[3]   Caputo, T.; Lisi, L.; Pirone, R.; Russo, G. Kinetics of the Preferential Oxidation of CO over CuO/CeO$_2$ Catalysts in H$_2$-rich Gases. *Ind. Eng. Chem. Res.* **2007**, *46*, 6793-6800.

[4]   Monte, M.; Gamarra, D.; López Cámara, A.; Rasmussen, S. B.; Gyorffy, N.; Schay, Z.; Martínez-Arias, A.; Conesa, J. C. Preferential Oxidation of CO in Excess H$_2$ over CuO/CeO$_2$ Catalysts: Performance as a Function of the Copper Coverage and Exposed Face Present in the CeO$_2$ Support. *Catal. Today* **2014**, *229*, 104-113.

[5]   Martínez-Arias, A.; Hungría, A. B.; Fernández-García, M.; Conesa, J. C.; Munuera, G. Preferential Oxidation of CO in a H$_2$-rich Stream over CuO/CeO$_2$ and CuO/(Ce,M)O$_x$ (M = Zr, Tb) Catalysts. *J. Power Sources* **2005**, *151*, 32-42.

[6]   Martínez-Arias, A.; Hungría, A. B.; Munuera, G.; Gamarra, D. Preferential Oxidation of CO in Rich H$_2$ over CuO/CeO$_2$: Details of Selectivity and Deactivation under the Reactant Stream. *Appl. Catal. B Environ.* **2006**, *65* , 207-216.

[7]   Mrabet, D.; Abassi, A.; Cherizol, R.; Do, T.-O. One-pot Solvothermal Synthesis of Mixed Cu-Ce-O$_x$ Nanocatalysts and Their Catalytic Activity for Low Temperature CO Oxidation, *Appl. Catal. A. Gen.* **2012**, *447– 448*, 60–66.

[8]   Moretti, E.; Lenarda, M.; Riello, P.; Storaro, L.; Talon, A.; Frattini, R.; Reyes-Carmona, A.; Jiménez-López, A.; Rodríguez-Castellón, E. Influence of Synthesis Parameters on the Performance of CeO$_2$–CuO and CeO$_2$–ZrO$_2$–CuO Systems in the Catalytic Oxidation of CO in Excess of Hydrogen, *Appl. Catal. B. Environ.* **2013**, *129*, 556–565.

[9]   Tang, X.; Zhang, B.; Li, Y.; Xu, Y.; Xin, Q.; Shen, W. Carbon Monoxide Oxidation over CuO/CeO$_2$ Catalysts. *Catal. Today* **2004**, *93-95*, 191-198.

[10]   Avgouropoulos, G.; Ioannides, T.; Matralis, H. Influence of the Preparation Method on the Performance of CuO–CeO$_2$ Catalysts for the Selective Oxidation of CO. *Appl. Catal. B. Environ.* **2005**, *56*, 87-93.

[11]   Liu, Z.; Zhou, R.; Zheng, X. Preferential Oxidation of CO in Excess Hydrogen over CuO-CeO$_2$ Catalyst Prepared by Chelating Method. *J. Nat. Gas Chem.* **2007**, *16*, 167-172.

[12] Liu, Z.; Zhou, R.; Zheng, X. Influence of Rare-earth Metal Doping on the Catalytic Performance of CuO-CeO$_2$ for the Preferential Oxidation of CO in Excess Hydrogen. *J. Nat. Gas Chem.* **2008**, *17*, 283-287.

[13] Reddy, L. H.; Reddy, G. K.; Devaiah, D.; Reddy, B. M. A Rapid Microwave-assisted Solution Combustion Synthesis of CuO Promoted CeO$_2$–M$_x$O$_y$ (M = Zr, La, Pr and Sm) Catalysts for CO Oxidation. *Appl. Catal. A. Gen.* **2012**, *445-446*, 297-305.

[14] Liu, W.; Flytzani-Stephanopoulos, M. Total Oxidation of Carbon Monoxide and Methane over Transition Metal Fluorite Oxide Composite Catalysts: I. Catalyst Composition and Activity. *J. Catal.* **1995**, *153*, 304–316.

[15] Liu, W.; Flytzani-Stephanopoulos, M. Total Oxidation of Carbon Monoxide and Methane over Transition Metal Fluorite Oxide Composite Catalysts: II. Catalyst Characterization and Reaction Kinetics. *J. Catal.* **1995**, *153*, 317–332.

[16] Avgouropoulos, G.; Ioannides, T.; Matralis, H.; Batista, J.; Hocevar, S. CuO–CeO$_2$ Mixed Oxide Catalysts for the Selective Oxidation of Carbon Monoxide in Excess Hydrogen. *Catal. Lett.* **2001**, *73*, 33–40.

[17] Hocevar, S.; Krasovec, U. O.; Orel, B.; Arico, A.; Lim, H. CWO of Phenol on Two Differently Prepared CuO–CeO$_2$ Catalysts. *Appl. Catal. B Environ* **2000**, *28*, 113–125.

[18] Zou, H.; Dong, X.; Lin, W. Selective CO Oxidation in Hydrogen-rich Gas over CuO/CeO$_2$ Catalysts. *Appl. Surf. Sci.* **2006**, *253*, 2893–2898.

[19] Yang, W., Li, D., Xu, D., Wang, X., Effect of CeO$_2$ Preparation Method and Cu Loading on CuO/CeO$_2$ Catalysts for Methane Combustion, *J. Nat. Gas Chem.* **2009**, *18*, 458-466.

[20] Avgouropoulos, G.; Ioannides, T. Selective CO Oxidation over CuO-CeO$_2$ Catalysts Prepared Via the Urea-nitrate Combustion Method. *Appl. Catal. A Gen.* **2003**, *244*, 155-167.

[21] Rattan, G., Prasad, R., Katyal, R.C., Effect of Preparation Methods on Al$_2$O$_3$ Supported CuO-CeO$_2$-ZrO$_2$ Catalysts for CO Oxidation, *Bull. Chem. React. Eng. Catal.* **2012**, *7*, 112-123.

[22] Mishra, A., Tripathi, B.D., Rai, A.K., Prasad, R., Comparative Study of Various Preparation Methods of CuO-CeO$_2$ Catalysts for Oxidation of n-Hexane and Iso-Octane, *Bull. Chem. React. Eng. Catal.* **2013**, *7*, 172-178.

[23] Gurbani, A.; Ayastuy, J. L.; Gonzalez-Marcos, M. P.; Gutierrez-Ortiz, M. A. CuO-CeO$_2$ Catalysts Synthesized by Various Methods: Comparative Study of Redox Properties. *Int. J. Hydrogen Energ.* **2010**, *35*, 11582-11590.

[24] Marban, G.; Fuertes, A. B. Highly Active and Selective CuO$_x$/CeO$_2$ Catalyst Prepared by a Single-step Citrate Method for Preferential Oxidation of Carbon Monoxide. *Appl. Catal. B Environ.* **2005**, *57*, 43–53

[25] Hu, T.; Yang, J.; Zhao, J.; Wang, D.; Song, H.; Chou, L. Preparation of a Cu–Ce–O Catalyst by Urea Combustion for Removing CO from Hydrogen. *Chinese J. Catal.* **2007**, *28*, 844-846.

[26] Cwele, T.; Mahadevaiah, N.; Singh, S.; Friedrich, H. B. Effect of Cu Additives on the Performance of a Cobalt Substituted Ceria (Ce$_{0.90}$Co$_{0.10}$O$_{2-\delta}$) Catalyst in Total and Preferential CO Oxidation. *Appl. Catal. B Environ.* **2016**, *182*, 1-14.

[27] Nguyen, T.-S.; Morfin, F.; Aouine, M.; Bosselet, F.; Rousset, J.-L.; Piccolo, L. Trends in the CO Oxidation and PROX Performances of the Platinum-group Metals Supported on Ceria. *Catal. Today* **2015**, *253*, 106-114.

[28] Di Benedetto, A.; Landi, G.; Lisi, L.; Russo, G. Role of CO$_2$ on CO Preferential Oxidation over CuO/CeO$_2$ Catalyst. *Appl. Catal. B Environ.* **2013**, *142-143*, 169-177.

[29] Patil, K.C.; Aruna, S.T.; Ekambaram, S. Combustion Synthesis. *Curr. Opin. Solid State Mater. Sci.* **1997**, *2*, 158–165.

[30] Kanervo, J. M.; Keskitalo, T. J.; Slioor, R. I.; Krause, A. O. I. Temperature-programmed Desorption as a Tool to Extract Quantitative Kinetic or Energetic Information for Porous Catalysts. *J. Catal.* **2006**, *238*, 382–393.

[31] Barbato, P. S.; Colussi, S.; Di Benedetto, A.; Landi, G.; Lisi, L.; Llorca, J.; Trovarelli, A. CO Preferential Oxidation under H_2-rich Streams on Copper Oxide Supported on Fe Promoted CeO_2, *Appl. Catal. A Gen.* **2015**, *506*, 268-277.

[32] Mistri, R.; Rahaman, M.; Llorca, J.; Priolkar, K. R.; Colussi, S.; Chandra Ray, B.; Gayen, A. Liquid Phase Selective Oxidation of Benzene over Nanostructured $Cu_xCe_{1-x}O_{2-\delta}$ ($0.03 \leq x \leq 0.15$). *J. Mol. Catal. A Gen.* **2014**, *390*, 187-197.

[33] Caputo, T.; Lisi, L.; Pirone, R.; Russo, G. On the Role of Redox Properties of CuO/CeO_2 Catalysts in the Preferential Oxidation of CO in H_2-rich Gases. *Appl. Catal. A Gen.* **2008**, *348*, 42-53.

[34] Martínez-Arias, A.; Fernández-García, M.; Soria, J.; Conesa, J.C. Spectroscopic Study of a Cu/CeO_2 Catalyst Subjected to Redox Treatments in Carbon Monoxide and Oxygen. *J. Catal.* **1999**, *182*, 367-377.

[35] Ammendola, P.; Barbato, P.S.; Lisi, L.; Ruoppolo, G.; Russo, G. Alumina Contribution to CO Oxidation: A TPR and IR Study. *Surf. Sci.* **2011**, *605*, 1812–1817.

[36] Martínez-Arias, A.; Gamarra, D.; Fernández-García, M.; Hornés, A.; Bera, P.; Koppány, Zs.; Schay, Z. Redox-catalytic Correlations in Oxidised Copper-ceria CO-PROX Catalysts, *Catal. Today* **2009**, *143*, 211-217.

[37] Colussi, S.; Gayen, A.; Farnesi Camellone, M.; Boaro, M.; Llorca, J.; Fabris, S.; Trovarelli, A. Nanofaceted Pd-O Sites in Pd-Ce Surface Superstructures: Enhanced Activity in Catalytic Combustion of Methane. *Angew. Chem. Int. Ed.* **2009**, *48*, 8481-8484.

[38] Landi, G.; Di Benedetto, A.; Colussi, S.; Barbato, P. S.; Lisi, L. Effect of Carbon Dioxide and Water on the Performances of an Iron-promoted Copper/ceria Catalyst for CO Preferential Oxidation in H_2-rich Streams, *Int. J. Hydrogen Energ.* **2016**, *41*, 7332-7341.
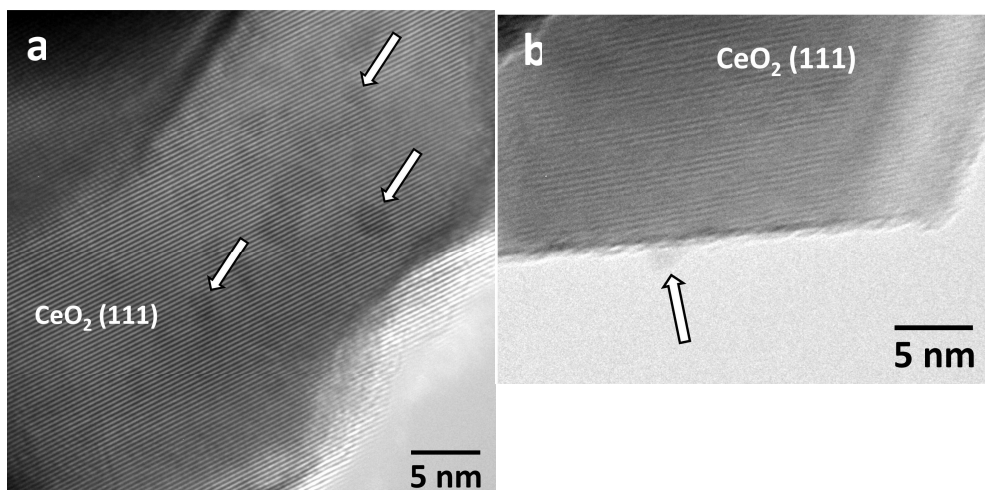
Figures
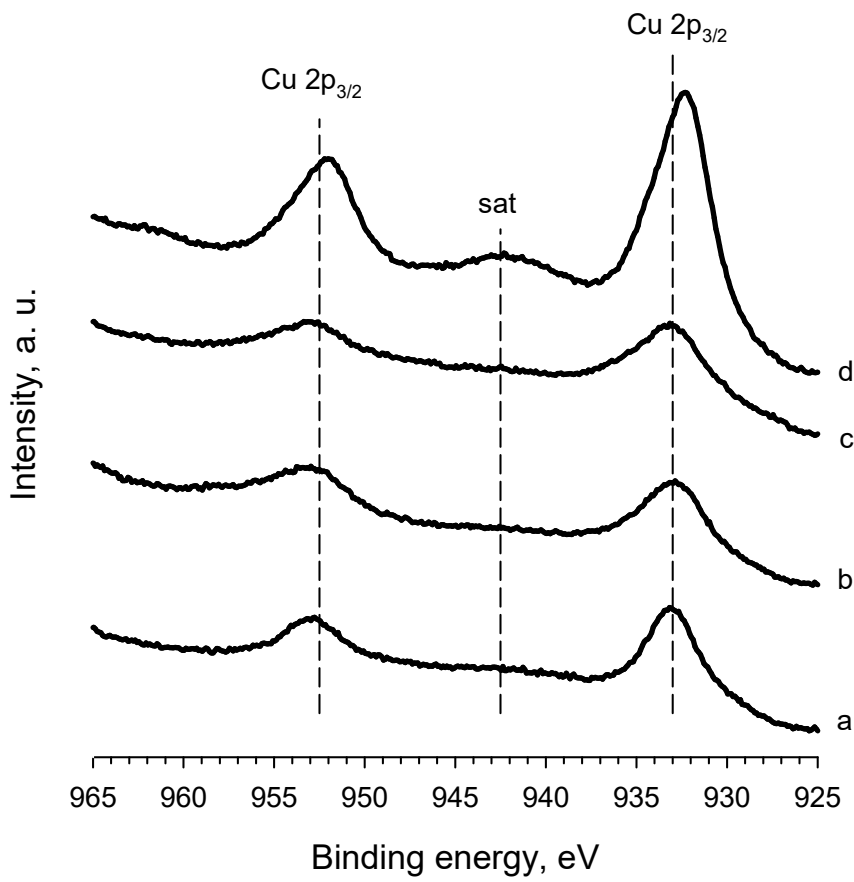
Figure 1. Cu 2p XPS spectra of CuCe-I (a: fresh, b: used) and CuCe-S (c: fresh, d: used) samples.
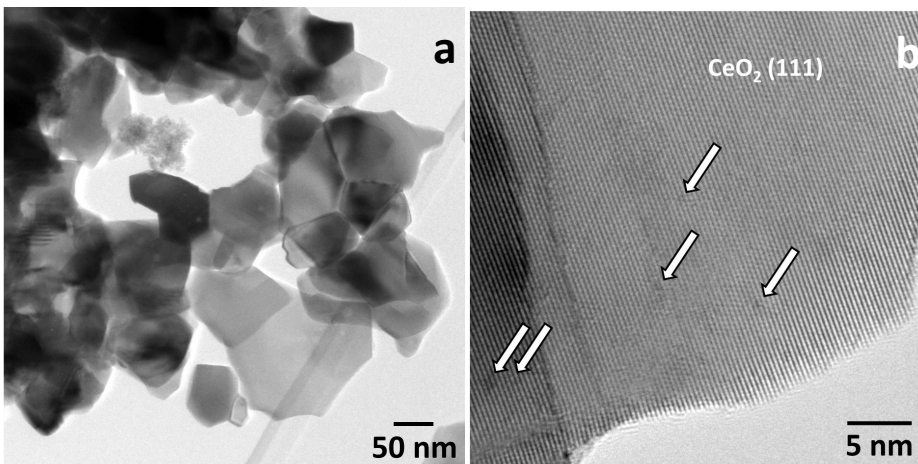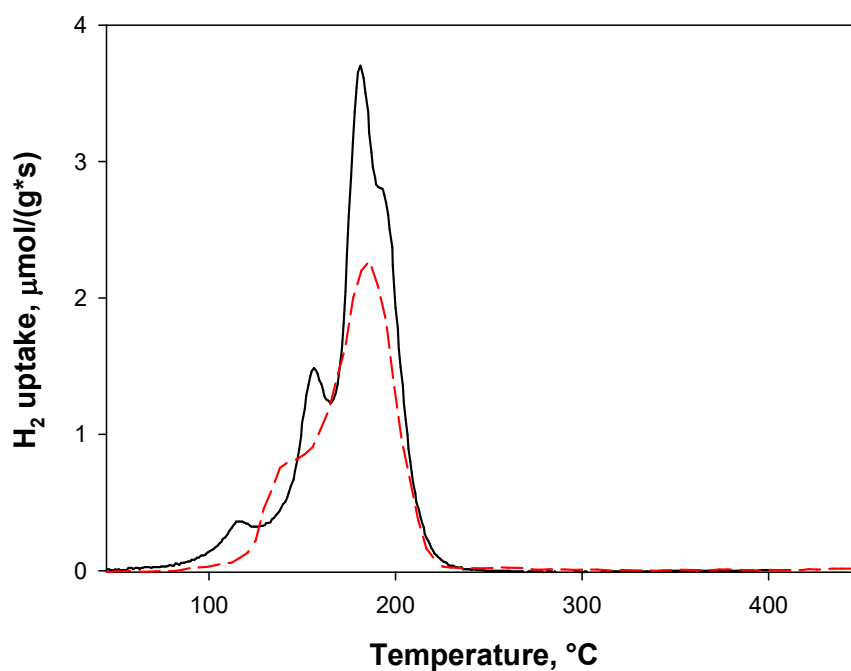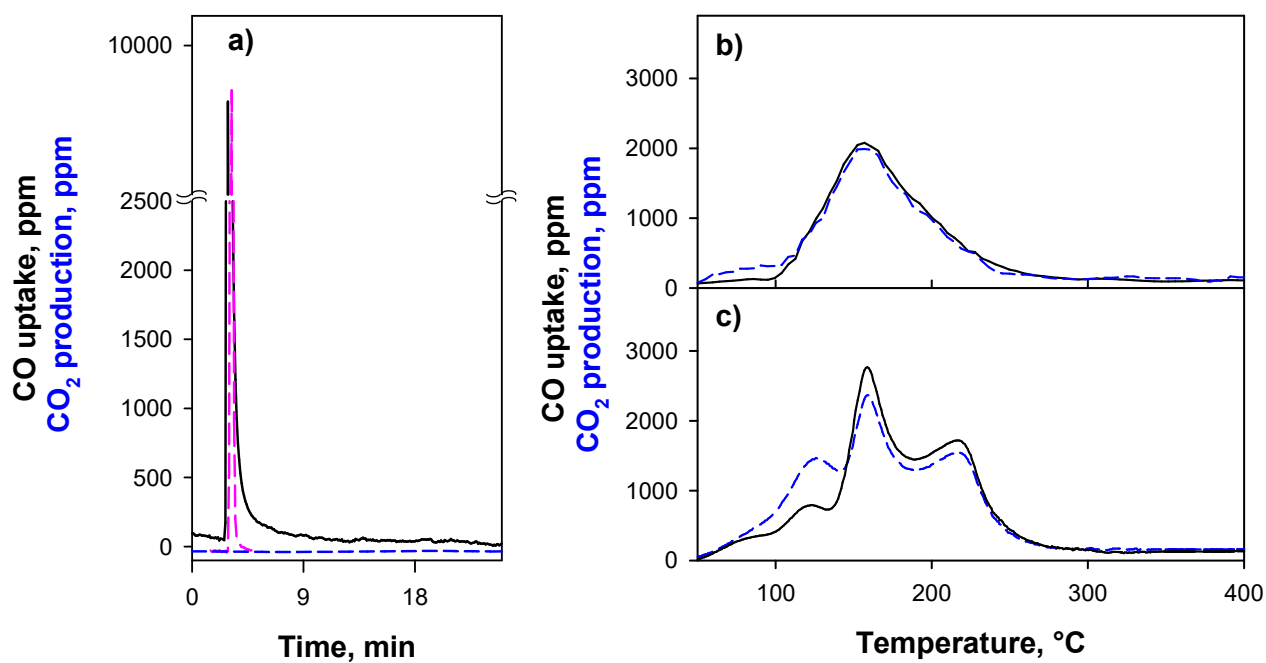
**Figure 2.** HRTEM images of the fresh CuCe-S sample: a) General view and b) High magnification**.**

Figure 3. HRTEM high magnification images of two different areas of the used CuCe-S sample**.**


Figure 4. H_2-TPR profiles: CuCe-S (red/dashed line); CuCe-I (black/solid line) adapted from Caputo el al.[31]

Figure 5. CO-TPR. a) CO consumption at room temperature on CuCe-S (the pink line represents the reactor hold-up). CO uptake (solid/black line) and CO_2 production (dashed/blue line) during CO TPR as a function of the temperature on CuCe-S (b) and CuCe-I (c) adapted from Caputo et al..[31]
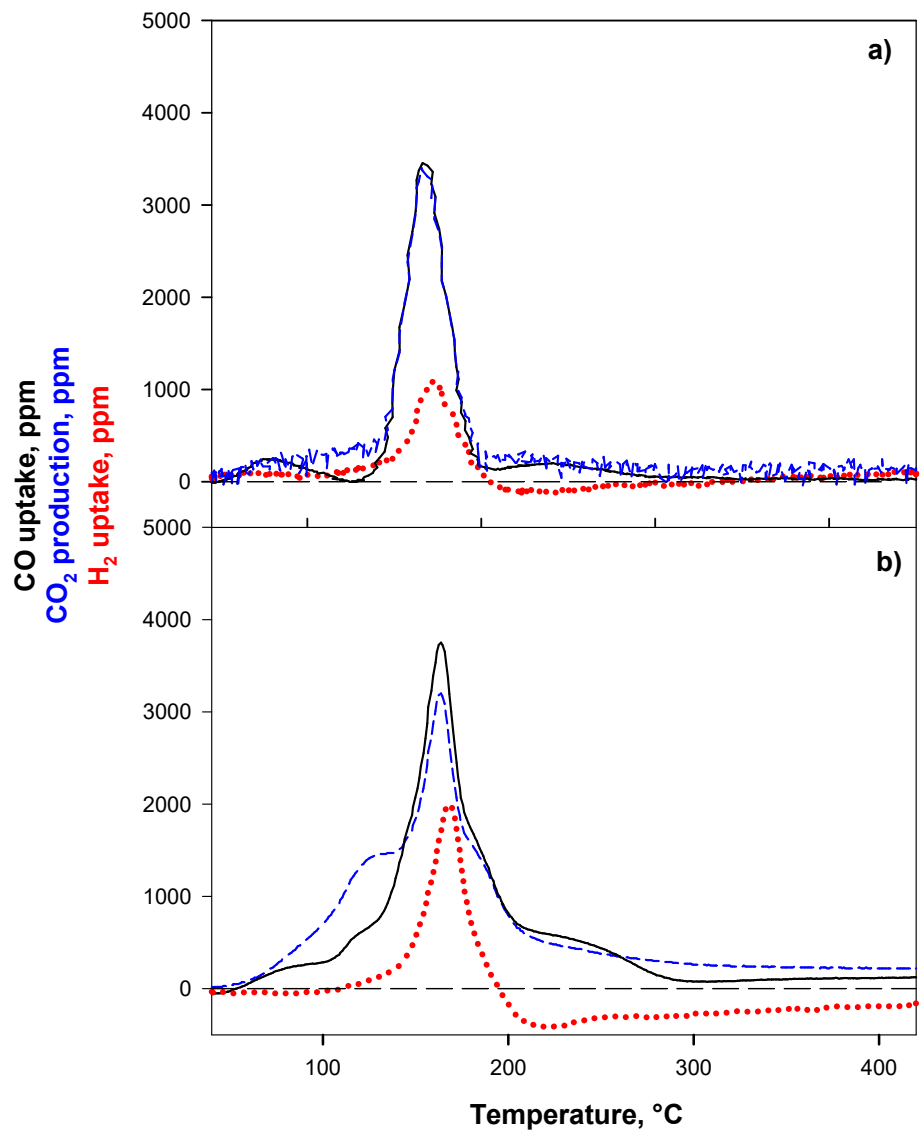
Figure 6. CO uptake (solid/black line), CO_2 production (dashed/blue line) and H_2 uptake (dotted/red line) during H_2-CO TPR on CuCe-S (a) and CuCe-I (b).
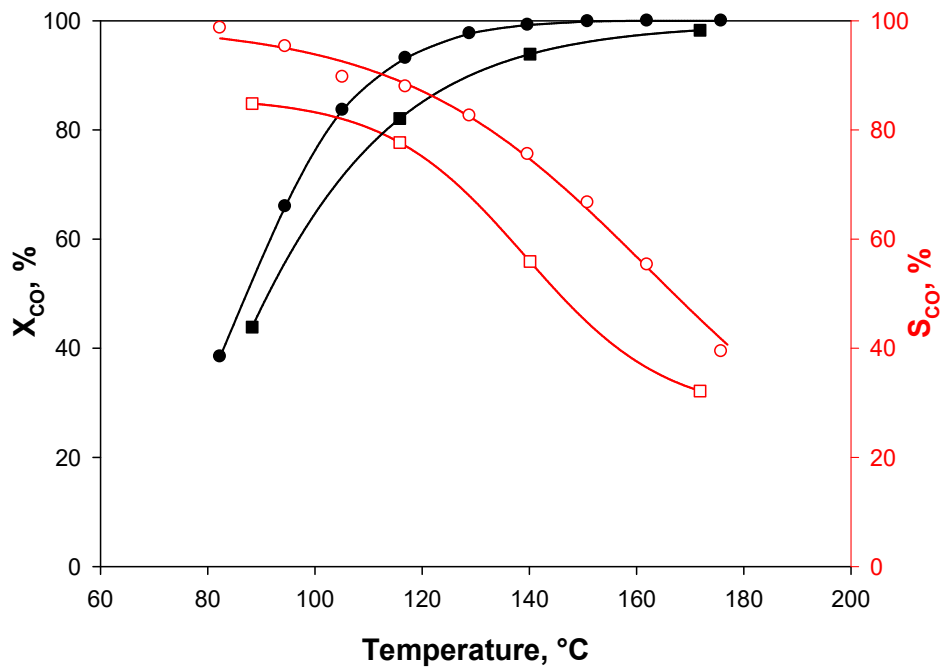
Figure 7. CO conversions (black/full symbols) and selectivities (red/open symbols) as a function of the temperature for the CuCe-S (circles) and CuCe-I (squares) catalysts. τ= 0.054 (g·s)·cm^{-3}; CO/H$_2$/O$_2$/N$_2$= 0.5/50/0.9/balance.
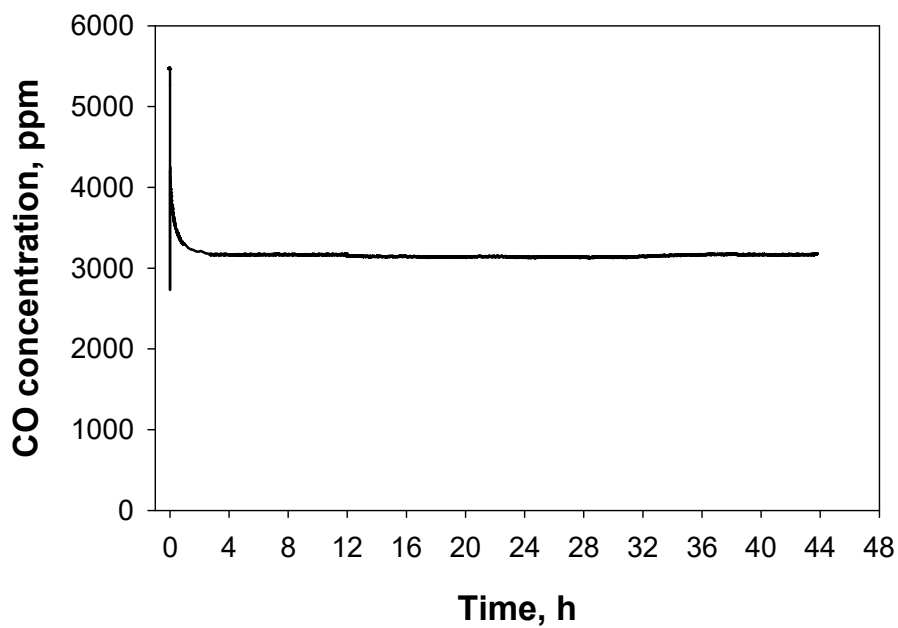
Figure 8. Outlet CO concentration as a function of the time on stream for the CuCe-S catalyst. τ= 0.054 (g·s)·cm^{-3}; Temperature: 80°C; CO/H$_2$/O$_2$/N$_2$= 0.5/50/0.9/balance.
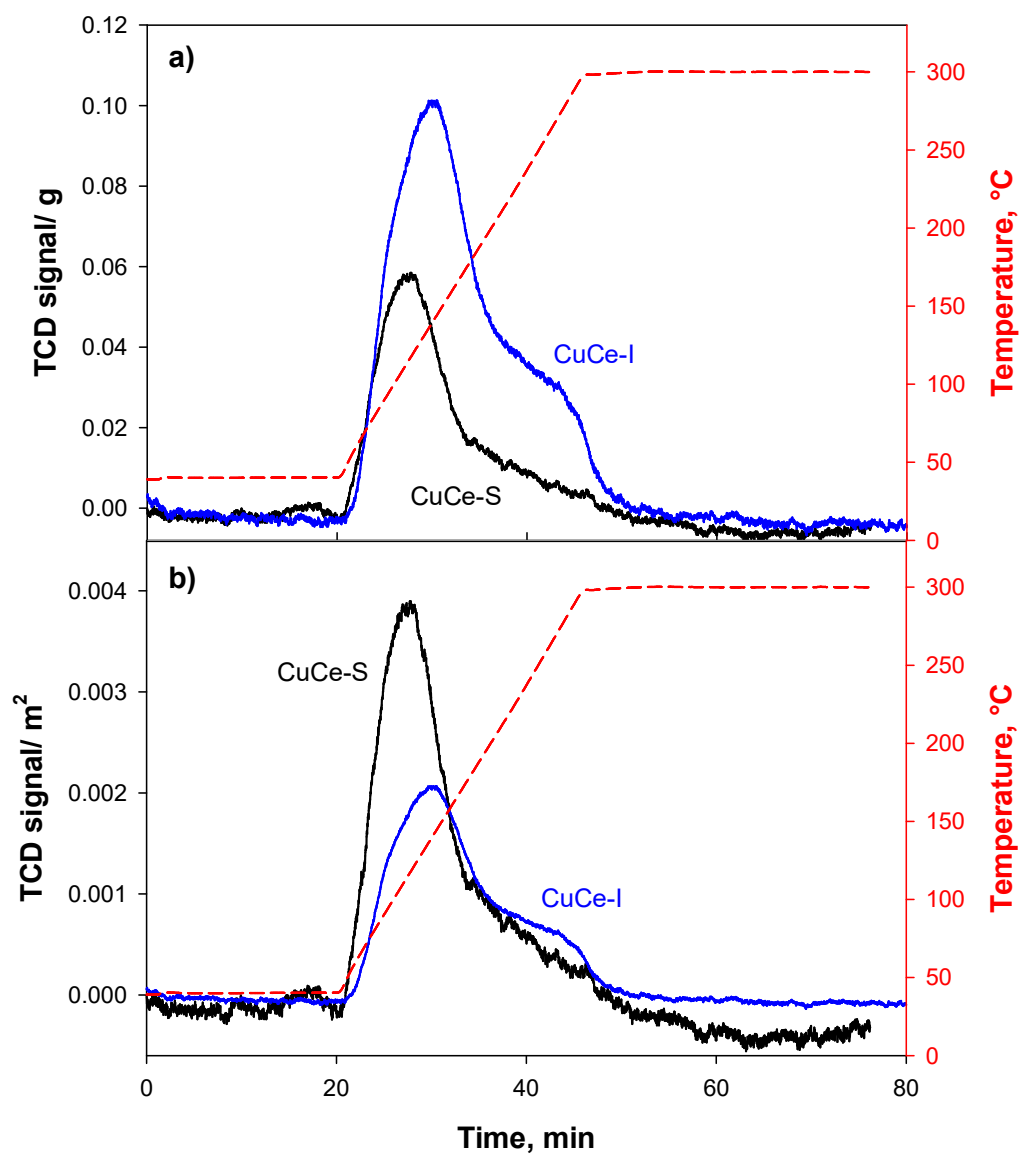
Figure 9. CO_2-TPD profiles over CuCe-S and CuCe-I. TCD signal as a function of time (a) per catalyst weight (g) and (b) per exposed surface area (m^2).
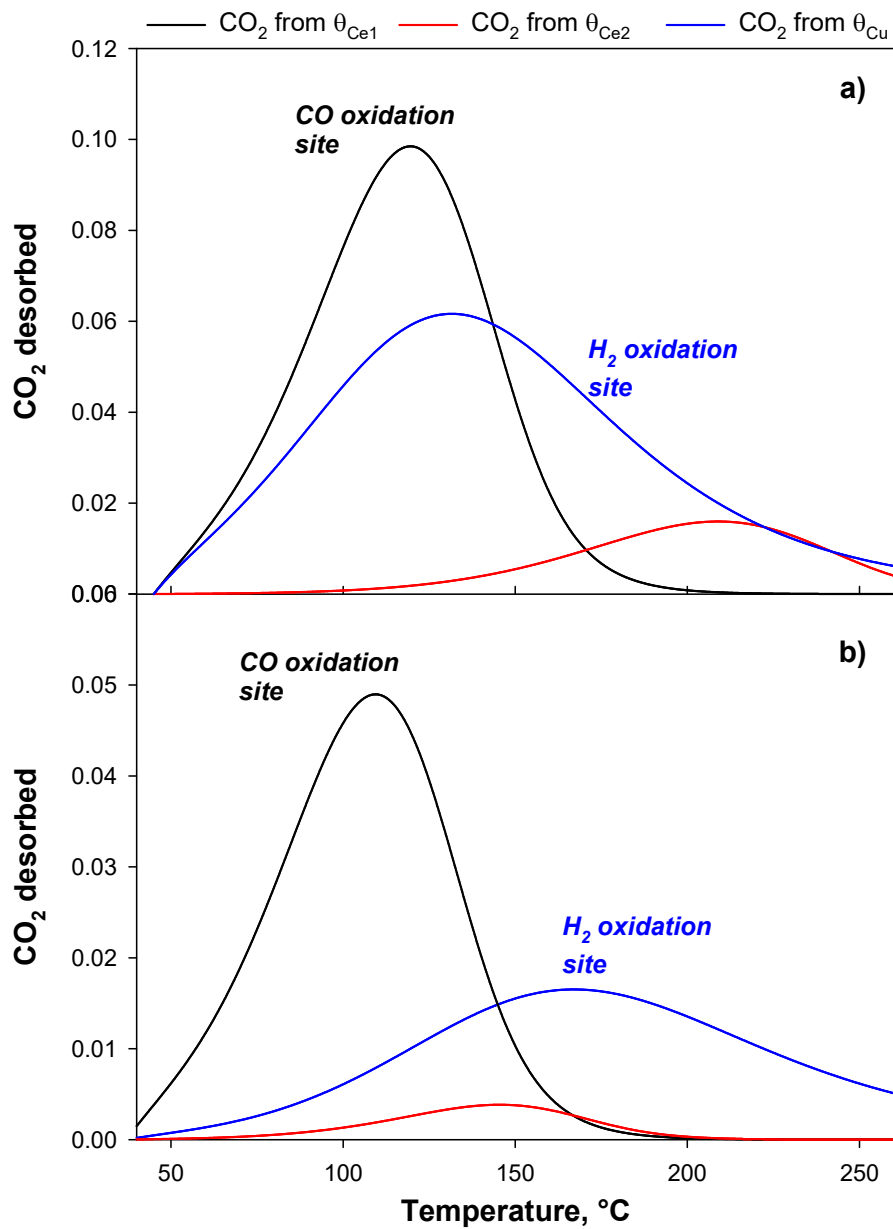
Figure 10. CO_2 desorbed from each site as obtained by the model over CuCe-I (a) and CuCe-S (b) catalysts.